frontiers | Frontiers in Earth Science

TYPE Original Research
PUBLISHED 22 February 2023
DOI 10.3389/feart.2023.1083030

Check for updates

OPEN ACCESS

EDITED BY
Jon Telling,
Newcastle University, United Kingdom

REVIEWED BY
Stephen A. Bowden,
University of Aberdeen, United Kingdom
Zhongping Li,
Chinese Academy of Sciences (CAS), China

*CORRESPONDENCE
Dujie Hou,
jiazhenjie0114@sina.com

SPECIALTY SECTION
This article was submitted to Geochemistry, a section of the journal Frontiers in Earth Science

RECEIVED 28 October 2022
ACCEPTED 13 February 2023
PUBLISHED 22 February 2023

CITATION
Jia Z, Hou D, Zhu X, Bian J and Ma X (2023), Organic geochemistry of Ordovician ultra-deep natural gas in the north Shuntuoguole area, Tarim Basin, NW China: Insights into genetic types, maturity, and sources.
Front. Earth Sci. 11:1083030.
doi: 10.3389/feart.2023.1083030

COPYRIGHT
© 2023 Jia, Hou, Zhu, Bian and Ma. This is an open-access article distributed under the terms of the Creative Commons Attribution License (CC BY). The use, distribution or reproduction in other forums is permitted, provided the original author(s) and the copyright owner(s) are credited and that the original publication in this journal is cited, in accordance with accepted academic practice. No use, distribution or reproduction is permitted which does not comply with these terms.

Organic geochemistry of Ordovician ultra-deep natural gas in the north Shuntuoguole area, Tarim Basin, NW China: Insights into genetic types, maturity, and sources

Zhenjie Jia[1,2,3], Dujie Hou[1,2,3]*, Xiuxiang Zhu[4], Jiejing Bian[1,2,3] and Xiaoxiao Ma[1,2,3]

[1]School of Energy Resources, China University of Geosciences, Beijing, China, [2]Key Laboratory of Marine Reservoir Evolution and Hydrocarbon Accumulation Mechanism, Ministry of Education, China University of Geosciences, Beijing, China, [3]Beijing Key Laboratory of Unconventional Natural Gas Geological Evaluation and Development Engineering, Beijing, China, [4]Northwest Oilfield Company, Sinopec, Urumqi, Xinjiang, China

As a gas-rich region in the Tarim Basin, the northern Shuntuoguole area (also known as the Shunbei area) is an attractive prospect. Non-etheless, the debate about the origins of these natural gas continues. The analysis on the geological context, natural gas components, and the carbon and hydrogen isotope ratios prove that methane is the predominate component of alkane gases. Alkane gases' carbon isotope fractionation ($\delta^{13}C_2 < -28‰$ and $\delta^{13}C_3 < -25‰$) shows that they are oil-associated gas, and their parent material type is I kerogen. Natural gas can be broken down further into three subgroups—Type I_1, Type I_2, and Type I_3. Based on the link between the carbon number 1/n and $\delta^{13}Cn$ of the gas. Modified plots of lnC_1/C_2 vs. lnC_2/C_3 reveal that kerogen cracking is the primary source of natural gas in the Shunbei area, and that this gas is combined with the contribution of oil cracking gas. Petroleum exploration and development in the Shunbei area can be justified on the basis that natural gas in the area originate primarily from Ordovician source rocks, as shown by carbon isotopic compositions.

KEYWORDS

natural gas, sources, isotopic composition, genetic types, Tarim Basin

1 Introduction

Globally there is great focus on exploring deep and ultra-deep gas fields (Dutton et al., 2010; Jia et al., 2015). As for the boundary depth of deep and ultra-deep petroliferous basins, the understanding of different countries, different institutions and different scholars in different periods is still quite different. Ultra-deep oil and gas reservoirs are distributed in two types of basins in the world, namely main rift basin and foreland basin. In foreland basin, ultra-deep oil and gas reservoirs are mainly distributed in foredeep tectonic belt (Huang B. J. et al., 2016). The world's deep oil and gas exploration began in the United States in the 1950s, and by the end of 2018, 68 oil and gas reservoirs with a depth of more than 8,000 m meters had been discovered worldwide (Jia et al., 2015).

At present, a large number of practices and researches have been carried out on the exploration of oil and gas in deep and ultra-deep basins in the world, and a series of major breakthroughs have been made. Especially, the three deepest wells in the world, namely Odoptu OP-11 Well in Sakhalin, Russia (12,345 m, in 2011), Ashosin Well in Qatar (12289 m in 2008) and SG-3 Well in kola peninsula (12,262 m in 1989) (Wu et al., 2006; Zhai et al., 2012), have obtained important information on deep oil and gas generation and reservoir properties. At present, the deepest drilling well in China is Luntan 1Well (8882 m, in 2019) in Tarim Basin, which can obtain high-yield industrial oil and gas flow in Cambrian below 8,200 m. Some industrial oil and gas reservoirs have also been found in Sichuan Basin and Tarim Basin in China in the depth range of 6,500–8,000 m (Pang et al., 2015), which shows that the ultra-deep still has good oil and gas exploration potential.

Natural gas, crude oil, and hydrocarbon source rocks in the Lower Paleozoic Ordovician and Cambrian reservoirs have been the subject of intense study since the discovery of the Shunbei Oilfield in China (Wang et al., 2003; He et al., 2008; Dai et al., 2014; Chen et al., 2015; Jiao, 2018; Zheng, 2018; Deng et al., 2019; Ma et al., 2020; Ma et al., 2021). However, the origin of these materials has been strongly contested (Zhu et al., 2015; Zhu et al., 2018; Qi, 2021). Palaeohigh in the Tarim Basin has been the target of petroleum exploration efforts in recent years. Insight into the strike-slip fault zone's tectonic history, structural features, active fault evolution process, and petroleum geological conditions has led to the growing understanding that it plays a crucial role in the formation of Tarim Basin's carbonate reservoirs and hydrocarbon accumulation (Zhang et al., 2021, 2019). A significant advancement in recent years has been the discovery of the Shunbei Oilfield (Zhao et al., 2018; Ma et al., 2019). This discovery has furthered the argument that intracratonic strike-slip faults with small displacements are crucial for reservoir development and hydrocarbon accumulation in the Ordovician carbonates (Qi, 2021). Deep oil and gas resources in China have great potential, and the exploration degree of oil and gas is low (13% and 10%, respectively). Deep and ultra-deep are the realistic fields for oil and gas exploration and development in the future (Jia et al., 2015; Pan et al., 2022). The research on the accumulation conditions and accumulation rules of the ultra-deep ancient strata has become a hot topic, and a number of high quality results have been obtained (Zhai and He, 2004; Bai et al., 2014; Ren et al., 2020; Li et al., 2021). It is of great significance to study the controlling effect of deep and ultra-deep natural gas geochemical characteristics on hydrocarbon accumulation and enrichment in order to guide the deep oil and gas exploration and development and meet the important national demand. In this study, we conducted a thorough investigation into the carbon and hydrogen isotopic compositions of the Ordovician natural gas in the Shunbei, and their geochemical properties.

2 Geological background

China's largest inland oil-gas yielding basin is located in the Tarim Basin, which is a large-scale superimposition basin. It is situated in Xinjiang, Northwest China, and has a size of around 560,000 square kilometers. Seven primary structural units plus a few subsidiary structural units make up the Tarim basin. Northern depression area is home to Shuntuoguole, which sits on secondary structural units. Accordingly, Shuntuoguole is subdivided into four tertiary structural units: the Shunbei gentle slope, the Shundong gentle slope, the Shuntuo low uplift, and the Shunnan gentle slope (Qi, 2021). The Shunbei Oilfield is located in the northern portion of the Shuntuoguole low uplift, and its near neighbors are the Shaya uplift to the north, the Kathak uplift to the south, the Awati depression to the west, and the Mangar depression to the east (Figure 1). From the perspective of tectonic evolution, the Tarim Basin has an ancient evolutionary history, which has undergone several subsidence and uplift movements on the plane. It is composed of seven tectonic evolution stages, and the evolution process is very complex (Jia, 1997). Substantial sedimentary layers, some of which are over ten thousand meters thick, and about 800 million years of geological history offer the material basis and objective conditions for the formation of oil and gas resources. Of these, 21 maritime oil and gas fields date back to the Paleozoic era, which is currently the focus of exploration and development (Jia, 1997; Zheng, 2018). To date, 18 main strike-slip faults have been found in the Tarim Basin, providing crucial information regarding the pattern of fault distribution. Overall structural characteristics of the Tarim Basin are governed by three fault types that can be categorized as NWW, NEE, or NNE (Jia, 1997; Deng et al., 2019). An important step forward was achieved in 2016 at the Shunbei Oilfield. Tarim basin has been a hotspot for petroleum exploration due to estimates that 18 strike-slip fault zones spanning 3,400 km^2 contain oil and gas with a total production of 1.7 billion tons, 70% of which is oil reserves, and natural gas reserves exceeding 5,000 cubic meters (Yang et al., 2017).

3 Materials and methods

The natural gas and crude oils samples were collected from the Ordovician Fault No. 7 (F7), Fault No. 5 (F5), Fault No.1 (F1) and Fault No.4 (F4) in the Shunbei area. The sample component is determined by HP5980 gas chromatograph. Chromatographic conditions were as follows: MS molecular sieve with column length of 2.4 mm; GDX-502 column of 4 m. The chromatographic temperature rise program is the initial temperature of 30°C, kept for 10 min, and then the temperature rise rate is 10°C/min to 180°C. The carbon isotope value of main alkane in natural gas is determined by Optima isotope mass spectrometer. Natural gas samples are separated into single components in HP5890 gas chromatograph by chromatographic column (HP-PLOTQ column). The natural gas sample was separated into a single component by a HP-PLOTQ column (30 m×0.32 mm×20 μm) in the HP5980 gas chromatograph. The single component hydrocarbons were converted into CO_2 by high temperature, and then directly entered the isotope mass spectrometer to determine the carbon isotope composition. The initial furnace temperature of the

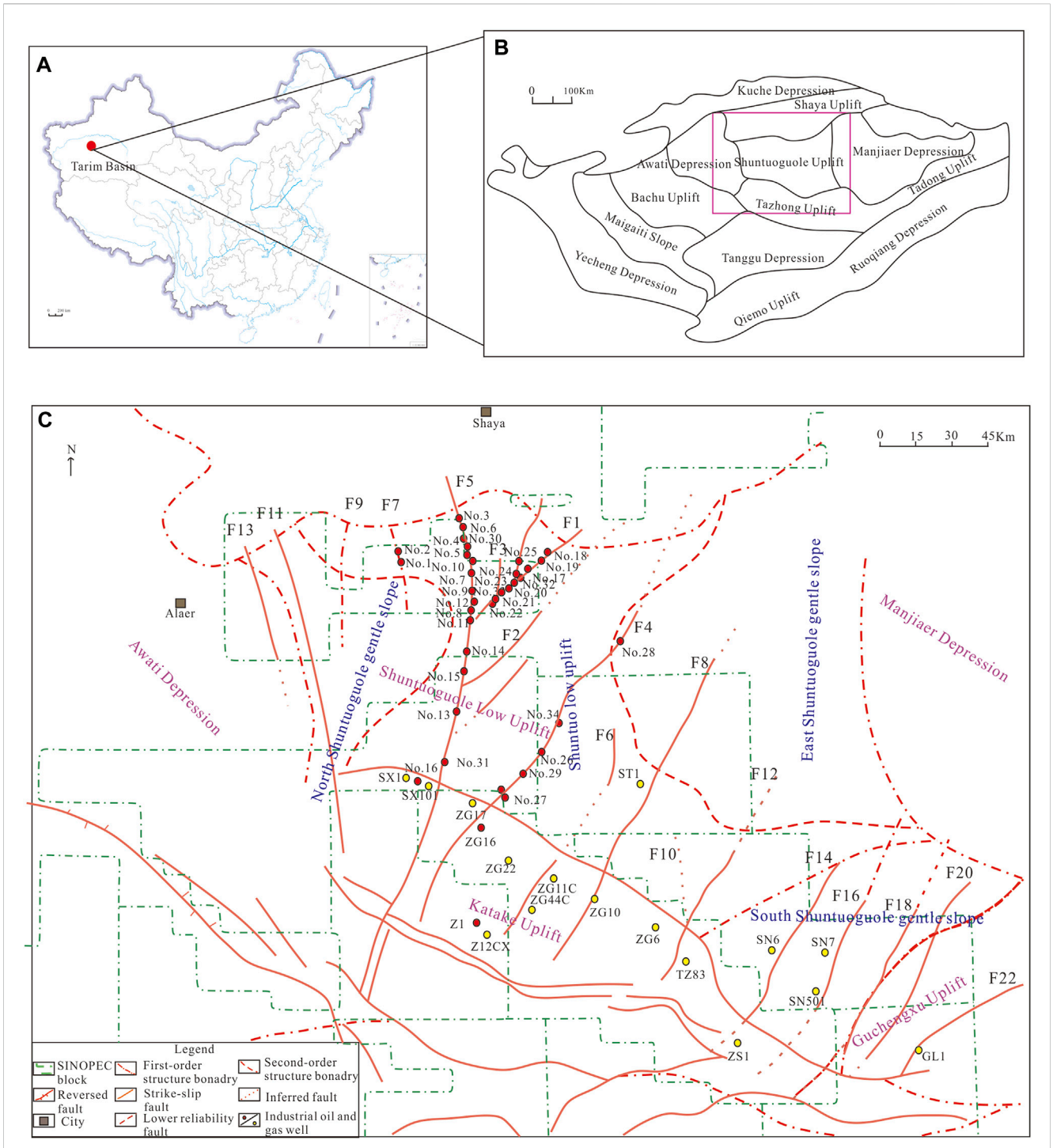

FIGURE 1
(A) location of the Tarim Basin in China and **(B)** location of the North Shuntuoguole area in Tarim Basin and **(C)** Map showing locations of the oilfield and some sampled wells and structure location of North Shuntuoguole area (Modified from Ma et al. 2021).

chromatograph is 35°C, and the temperature rise rate is 8°C/min to 80°C, and the temperature rise rate is 5°C/min to 260°C, and the temperature rise is maintained for 10 min. The CO_2 experiment utilized a PorparKQ column (2 m×3 mm) with Helium as the carrier gas. The temperature of the GC column was raised from 40 to 100°C in one-minute increments. It took a TDX column (2 m×3 mm) heated at a rate of 20°C per minute from 32°C to 120°C to separate the remaining gases that are not hydrocarbons. By comparing the results to the PDB carbon isotope, the precision of the analysis was found to be ±0.5‰. All the above tests were completed in Sinopec Key Laboratory of Petroleum Accumulation (Wuxi). Using the relationship between Ro and $\delta^{13}C1$, $\delta^{13}C1=21.88\log Ro-45.6$, the corresponding Ro value is obtained.

TABLE 1 Molecular and stable carbon isotopic compositions of natural gases from Shunbei area.

Fault no.	Well no.	Components/%							$\delta^{13}C$/‰(VPDB)%				$\delta^{13}H$/‰(VSMOW)%				
		H_2	N_2	CO_2	CH_4	C_2H_6	C_3H_8	C_1/C_{1+5}	CO_2	CH_4	C_2H_6	C_3H_8	CH_4	C_2H_6	C_3H_8	Ro	
F7	1	0.15	9.31	8.99	47.92	17.83	10.85	0.61	−5	−46.4	−37.7	−33.2	−208	−205	−152	0.92	
	2	0.76	1.85	6.90	46.89	20.92	14.78	0.52	−14	−48.4	−39	−33.9	n.d.	n.d.	n.d.	0.74	Quoted from Ref Ma et al. (2021)
F5 North	3	0.03	11.34	6.79	58.67	14.54	6.17	0.72	−7.8	−49.2	−39.1	−35.1	−205	−185	−157	0.68	
	4	0.18	5.84	8.06	54.48	17.97	9.43	0.63	−3.7	−48.9	−39.3	−35.6	−207	−180	−141	0.71	
	5	0.02	n.d.	30.00	12.57	17.29	21.56	0.19	−2.5	−49.2	−38.6	−34.1	−217	−173	−133	0.68	
	6	0.19	2.36	5.05	62.06	18.00	8.70	0.67	−2	−49	−37.7	−34.1	n.d.	n.d.	n.d.	0.70	Quoted from Ref Ma et al. (2021)
F5 Middle	7	n.d.	n.d.	68.21	13.64	9.09	4.55	0.43	−9.9	n.d.	n.d.	n.d.	n.d.	n.d.	n.d.	n.d.	
	8	0.19	n.d.	47.80	47.57	2.96	0.81	0.92	n.d.	n.d.	n.d.	n.d.	n.d.	n.d.	n.d.	n.d.	
	9	0.01	1.10	6.11	31.15	25.50	19.59	0.82	−4	−48	−33.83	−31.3	−188	−144	−123	0.78	
	10	0.01	3.82	1.65	80.14	9.34	3.49	0.85	1.2	-47.8	−33.6	−30.9	−182	−131	−110	0.79	
	11	0.01	4.18	2.07	82.21	8.36	2.41	0.88	−1.1	-47.5	−33.5	−30.7	−182	−128	−102	0.82	
	12	0.02	2.52	2.15	83.25	8.15	2.73	0.88	−0.5	-47.6	−33.3	−30.6	−180	−127	−102	0.81	
F5 South	13	0.14	1.71	5.79	87.90	3.21	0.66	0.95	−9	-47.5	−28.6	−25.4	n.d.	n.d.	n.d.	0.82	
	14	0.04	0.87	19.05	74.43	3.57	1.03	0.93	−4.1	-47.3	−32.1	−29.3	n.d.	n.d.	n.d.	0.84	
	15	0.06	4.96	6.49	74.51	7.90	3.08	0.84	−13.8	−47.7	−33.4	−31.7	−159	n.d.	n.d.	0.80	Quoted from Ref Ma et al. (2021)
	16	0.01	n.d.	8.30	84.91	3.12	1.20	0.94	2.7	−51.7	−32.5	−28.2	n.d.	n.d.	n.d.	0.53	
F1 North	17	0.32	1.55	11.01	84.18	2.43	0.41	0.97	n.d.	−44.7	−33.1	−30.8	−174	−129	−116	1.10	Quoted from Ref Ma et al. (2021)
	18	0.01	1.16	2.59	83.73	6.99	3.25	0.87	0.1	−44.7	−33.3	−30.8	n.d.	n.d.	n.d.	1.10	
	19	0.17	1.82	6.87	77.37	8.15	3.55	0.86	−2.8	−46	−34.4	−32.1	−162	−111	−105	0.96	
	20	n.d.	2.20	2.32	80.35	9.05	3.98	0.85	0.5	−47	−33.8	−31.6	−180	−148	−116	0.86	
	21	1.58	2.53	16.36	67.76	7.45	2.54	0.86	−1.6	−48.1	−34.8	−32.3	−178	n.d.	n.d.	0.77	
F1 South	22	0.05	3.05	4.43	77.36	10.11	3.61	0.84	−5.9	−48.8	−34.7	−32.2	−162	−110	−101	0.71	Quoted from Ref. Ma et al. (2021)
	23	0.02	1.99	6.75	78.12	8.32	3.16	0.86	−6.4	−46.6	−34.1	−32	−156	−113	−104	0.90	
F1 Splay	24	0.54	1.81	10.43	74.04	7.82	3.38	0.86	−1.4	−47.2	−33.8	−31.2	−169	−111	−107	0.85	
	25	0.02	1.22	3.73	74.57	9.02	5.81	0.81	−2.85	−46.6	−34.15	−31.9	−167	−119	n.d.	0.90	
F4	26	0.26	1.93	8.96	86.15	1.91	0.50	0.97	−6.7	−44.2	−29.9	−27.5	−151	−99	−81	1.16	
	27	0.17	0.37	16.16	77.70	3.49	1.10	0.94	−4.7	−47.4	−34.4	−29.8	n.d.	n.d.	n.d.	0.83	
	28	0.04	0.51	6.60	80.65	7.30	2.71	0.88	−7	−45.7	−33.7	−30.9	n.d.	n.d.	n.d.	0.99	

(Continued on following page)

TABLE 1 (*Continued*) Molecular and stable carbon isotopic compositions of natural gases from Shunbei area.

Fault no.	Well no.	Components/%							δ^{13}C/‰(VPDB)%				δ^{13}H/‰(VSMOW)%				
		H_2	N_2	CO_2	CH_4	C_2H_6	C_3H_8	C_1/C_{1+5}	CO_2	CH_4	C_2H_6	C_3H_8	CH_4	C_2H_6	C_3H_8	Ro	
	29	n.d.	n.d.	n.d.	n.d.	n.d.	n.d.	n.d.	n.d.	n.d.	n.d.	n.d.	−146	−99	n.d.	n.d.	

Note: n.d.: no data.

TABLE 2 Carbon isotope for Cambrian source rock extracts, typical Cambrian oils and typical Ordovician oils from the Tarim Basin.

	Wells	Depth/m	Strata	$\delta^{13}C_{PDB}$ (‰)				
				SAT	ARO	RES	ASPH	
Ordovician oils in Shunbei	No.1	7,674-8,024.66	O	−30.70	−30.00	−29.60	−30.00	
	No.30	n.d.	O	−32.50	−30.90	−30.30	−31.20	
	No.14	8,050	O_{2yj}-O_{1-2y}	−32.90	−31.20	−31.00	−32.30	
	No.31	7,438.42	O_{2yj}-O_{1-2y}	−29.50	−28.80	−29.00	−29.30	
	No.32	7,458-7,613.05	O2yj	−32.80	−30.70	−28.80	−29.30	
	No.33	n.d.	O	−32.80	−31.70	−30.40	−30.00	
	No.34	7,531	O_{2yj}-O_{1-2y}	−31.00	−30.00	−29.30	−28.60	
Cambrian source rocks in Tarim basin	KN1	4,994	$\epsilon_3$ql	n.d.	n.d.	n.d.	n.d.	Quoted from Ref. Song et al. (2016) and Yang et al. (2017)
	KN1	5,188	$\epsilon_3$ql	n.d.	n.d.	n.d.	n.d.	
	H4	4,598-4,599	$\epsilon_3$ql	−27.00	−25.80	−26.50	−26.40	
	TD2	4,772	ϵ_3t	n.d.	n.d.	n.d.	n.d.	
	YL1	4,228	ϵ_2m	−27.00	−26.20	−27.20	−28.20	
	KN1	5,188.5	ϵ_3	−28.90	−28.00	−27.50	−28.70	
	TD2	4,919.2	ϵ_1	−28.8	−28	−28.3	−28.5	
	YL1	4,235	ϵ_2m	n.d.	n.d.	n.d.	n.d.	
	XH1	5,826–5,830	ϵ_1y	n.d.	n.d.	n.d.	n.d.	
Cambrian oils in Tarim basin	TZ26	4,392–440	O_3l	n.d.	n.d.	n.d.	n.d.	Quoted from Ref. Song et al. (2016) and Yang et al. (2017)
	T904	5,900–5,935	O_1y	−29.70	−28.70	−28.30	n.d.	
	LK1	4,265–4,305	J	n.d.	n.d.	n.d.	n.d.	
	MA4-2	2017-2041	O_3l	n.d.	n.d.	n.d.	n.d.	
	TD2	4,561–5,040	ϵ	−29.30	−28.10	−27.90	−27.40	

Note: SAT= saturated; ARO= aromatics; RES= resins; ASPH= asphaltene.

4 Results

4.1 Molecular composition of natural gas

Natural gas's constituents are a crucial indicator of the genetic types of natural gas that are present. Given that hydrocarbons, which make up more than 70% of the total gas and dominate the molecular composition of the natural gas in the study area, the natural gas are likely mostly derived from organic sources, according to this theory. Methane is the main hydrocarbon gas in natural gas, and the methane content ranges from 12.57% to 87.90% (Table 1), with an average of 67.3%, the main peak

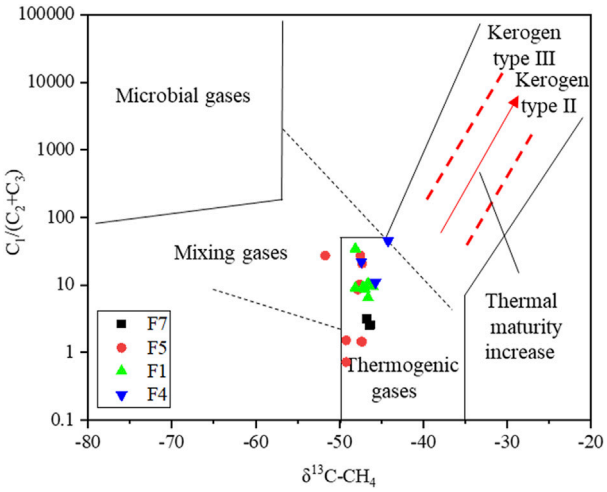

FIGURE 2
Plot of $\delta^{13}C–CH_4$ vs. $C_1/(C_2+C_3)$ values of natural gases from the Shunbei area (Modified from Bernard 1978).

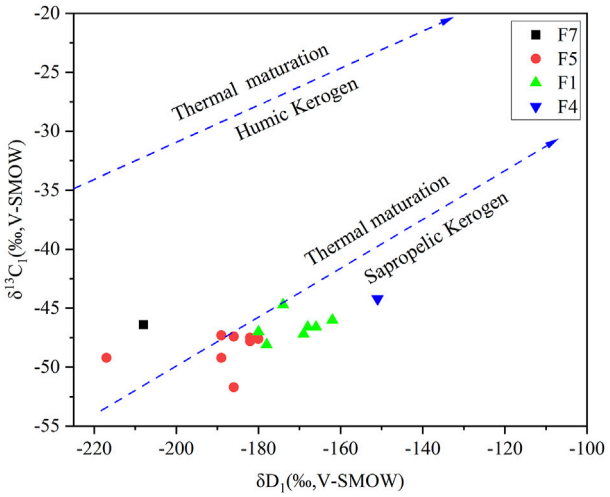

FIGURE 3
Generalized summary plots of δD –CH_4 vs. $\delta^{13}C$ –CH_4 for the natural gases from Shunbei area (Modified from Wang et al., 2015).

between 70% and 90%. The minor ethane content varies between 1.91% and 25.50%, with an average of 9.64%; the trace propane content varies between 0.41% and 21.56%, with an average of 5.18%; and Well No.13 has the highest concentration, at 87.90%. Well No.5 has the lowest concentration, at 12.57%. Natural gas's dryness indices ($C_1/C_{1\text{-}5}$) range from 0.19% on the low end to 0.97% on the high end, with an average of 0.8% (which is typical for wet gas) across faults (Table 1). Nitrogen (N_2), carbon dioxide (CO_2), and hydrogen (H_2) are the most common non-hydrocarbon gases in Shunbei's natural gas, albeit at low amounts. The CO_2 content ranges from 1.65% to 68.21% (11.77% on average), with the majority of the CO_2 content being less than 10% (Table 1). The N_2 content ranges from 0.37% to 11.34% (2.92% on average) (Table 1), with the majority of the N_2 content being around 2%; and the H_2 content ranges from 0.01% to 1.58% (0.19% on average) (Table 1).

4.2 Carbon and hydrogen isotopes of natural gas

Natural gas in the research area has a standard stable carbon isotope trend, with methane ($\delta^{13}C_1$), ethane ($\delta^{13}C_2$), and propane ($\delta^{13}C_3$) carbon isotope levels increasing with increasing carbon number, starting at a value of −51.7‰ to −44.2‰ (average −47.43‰), −39.3‰ to −28.6‰ (average −34.47‰), −35.6‰ to −25.4‰ (average −31.43‰), respectively. Carbon dioxide ($\delta^{13}C_{CO2}$) has a $\delta^{13}C$ value that varies from 14 to 2.7‰ (Table 1). The natural gas in the study area has the methane hydrogen isotope ($\delta^2H–CH_4$) values rang from −217‰ to −146‰ (average −177‰), the ethane hydrogen isotope ($\delta^2H–C_2H_6$) values rang from −205‰ to −99‰ (average −133‰), and the propane carbon isotope ($\delta^2H–C_3H_8$) values rang from −157‰ to −81‰ (average −116‰) (Table 1).

5 Discussion

5.1 Genetic types and origins of natural gas

Oil and gas' geochemical properties are mostly determined by their parent material, degree of maturation, and other processes. Natural gas formation theories center mostly on the peculiarities of light hydrocarbons and various isotopes of carbon and hydrogen. ^{12}C is typically enriched in the low molecular hydrocarbon as a result of organic matter breaking, whereas ^{13}C is significantly enriched in the large molecular hydrocarbon, such that the carbon isotope ratios of natural gas components are ordered from small to large ($\delta^{13}C_1 < \delta^{13}C_2 < \delta^{13}C_3 < \delta^{13}C_4$). The difference in carbon isotope content between neighboring components correlates with the age of the parent rock. When the maturity is low, the difference of carbon isotope is obvious. Differences tend to decrease and sometimes reverse as maturity increases ($\delta^{13}C_1 > \delta^{13}C_2 > \delta^{13}C_3 > \delta^{13}C_4$) (Schoell 1980; Whiticar et al., 1986; Whiticar 1999; Dai et al., 2016; Xie et al., 2017; Ni et al., 2019). Therefore, the carbon isotope ratio index can be adopted to determine the origin and genetic makeup of various parent natural gases at various times in their development. Carbon isotope characteristics of ethane and propane, as well as the geological history of the study area, suggest that the natural gas in the Shunbei area are likely thermogenic gases (Figure 2). Methane's hydrogen isotopic composition varies with its sedimentary context, and this variation can be used as a valuable indication of that environment. For methane, the concentration of hydrogen isotopes is highest in marine environments rich in salt, followed by those rich in brackish water and finally those rich in fresh water. The value of methane hydrogen isotope is bounded by −180‰, when the value more than −180‰, indicating marine source rocks; otherwise, indicating continental source rocks (Wang et al., 2015). The average δD–CH_4 values of the naturally occurring gases in Fault 7, 5, 1, and 4 are −208‰, −190‰, and −168.5‰, and −148.5‰, respectively (Table 1). The carbon and hydrogen

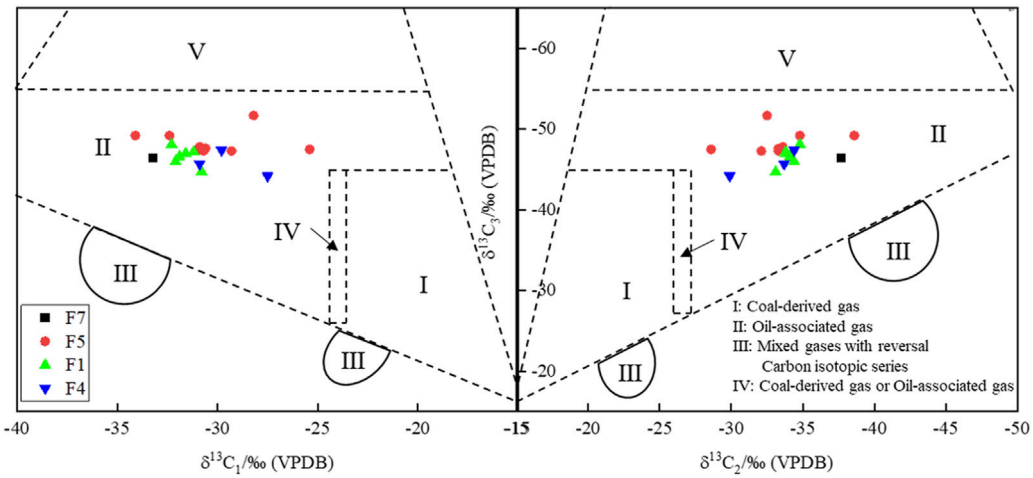

FIGURE 4
Genetic identification of alkane gases showing that the natural gases from the Shunbei area along the exhibits the characteristics of oil-associated gas (Modified from Dai et al., 1992).

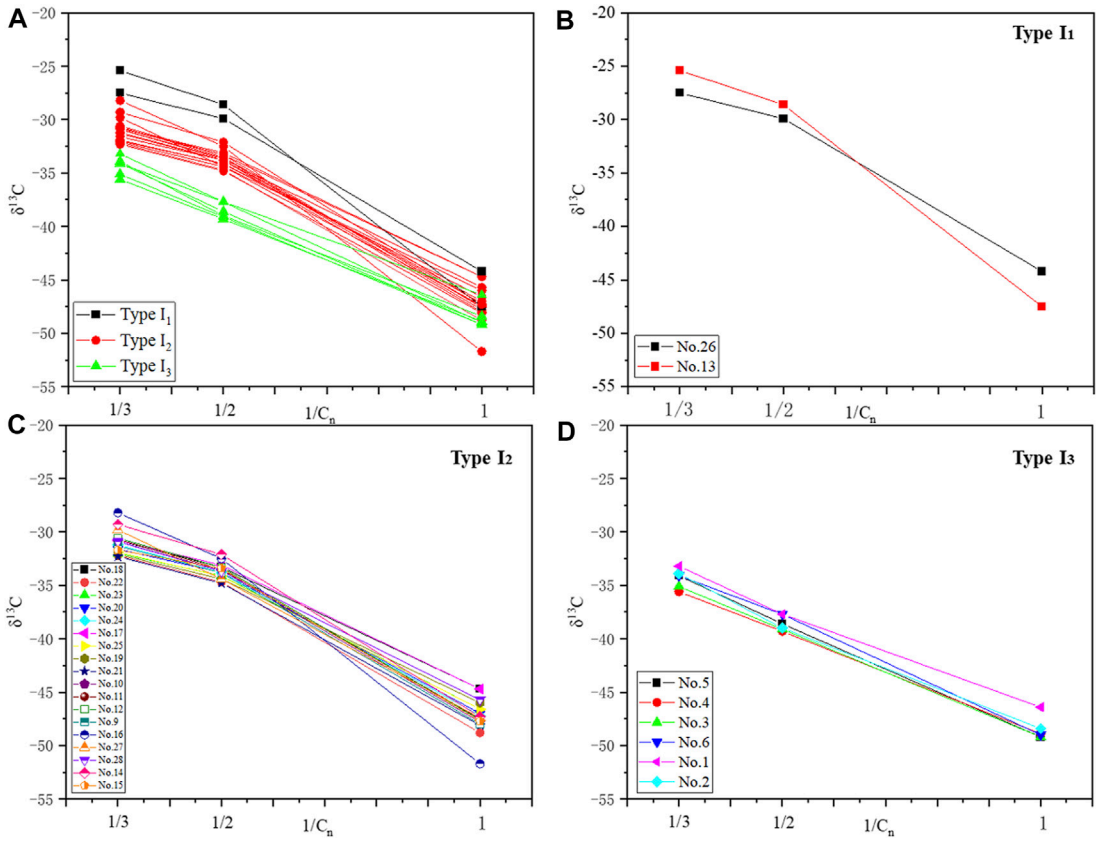

FIGURE 5
Relationship between carbon number 1/n and δ^{13}Cn of natural gases in Shunbei **(A)** Classification of natural gas types in Shunbei and **(B)** Type I_1 natural gases and **(C)** Type I_2 natural gases and **(D)** Type I_3 natural gases (Modified from Chung et al., 1988; Dai et al., 2003).

isotope properties of methane are used to identify the origin of natural gas, and these measurements showed that the gases in the research area were consistent with a sapropelic-kerogen source (Figure 3). To more accurately determine the genetic types of natural gases based on their isotopic makeup, scientists have discovered that carbon isotopes may be utilized to distinguish

between gas originating from coal and gas related with oil. Researchers in Shunbei could tell that the gas was predominantly from zone II and that it was an oil-associated gas by analyzing its carbon isotope composition (Figure 4).

Natural gas genetic kinds can be determined using carbon isotopes contained in gas components as trustworthy indicators. In order to gauge the precision of the method, the reciprocal value of the carbon number associated with methane and pentanes is used (Chung et al., 1988; Dai et al., 2016). In the case when δ^{13}Cn is proportional to 1/n, it can be inferred that the carbon isotopic composition of the ancestor is also homologous. However, if this is not the case, it suggests that the genetic source has a complex carbon isotope makeup (Prinzhofer et al., 1995; Zhang et al., 2005; Zou et al., 2007). In the Shunbei, there is a positive trend in the carbon isotopic compositions of alkanes, suggesting that these gases are produced by the cracking of organic materials. This is denoted by the notation $\delta^{13}C_1 < \delta^{13}C_2 < \delta^{13}C_3$. According to the information presented in Table 1, $\delta^{13}C_1$ and $\delta^{13}C_2$ values of natural gases display quite wide ranges of variation, with values ranging from −51.7‰ to −44.2‰ (average −47‰) and −39.3‰ to −28.6‰ (average −34‰), respectively. Natural gases are oil-associated gas and its parent material type is I kerogen in Shunbei, which can be further divided three subcategories. Type I_1, Type I_2 and Type I_3 (Figure 5A). Type I_1 shows a positive trend, $\delta^{13}C_1$ values range from −47.5‰ to −44.2‰ (average −45.85‰), $\delta^{13}C_2$ values range from −28.6‰ to −29.9‰ (average −29.3‰) (Table 1; Figure 5B), the representative wells are No. 26 and No. 13, and $C_1/\Sigma C_{1-5}$ values range from 0.97 to 0.95, respectively, indicating dry gas and oil-associated gas of high maturity. Type I_2 shows a positive trend, $\delta^{13}C_1$ values of the Type I_2 range from −51.7‰ to −44.7‰ (average −47.2‰), $\delta^{13}C_2$ values of the Type I_2 range from −34.8‰ to −32.1‰ (average −33.7‰) (Table 1; Figure 5C). $C_1/\Sigma C_{1-5}$ values of Type I_2 range from 0.81 to 0.97 (average 0.87), the Type I_2 gas is wet gas. The $\delta^{13}C_1$ values of the Type I_3 range from −49.2‰ to −46.4‰ (average −48.51‰), $\delta^{13}C_2$ values of the Type I_3 range from −39.3‰ to −37.7‰ (average −38.6‰) (Table 1; Figure 5D). $C_1/\Sigma C_{1-5}$ values of Type I_3 range from 0.19 to 0.72 (average 0.56), the Type I_3 gas is wet gas. Type I_2 and Type I_3 gases are distinguished from Type I1 gases by having $\delta^{13}C_3$ values typically lower than −28.0‰. In addition, Type I_1 gas exhibits heavier $\delta^{13}C_3$ values than Type I_2 and Type I_3 gas, indicating a greater degree of thermal maturity.

5.2 Carbon dioxide

Although CO_2 is widely distributed in nature, its concentration is generally low. If located near to oil fields, large reserves of CO_2 have the potential to be used to enhance oil recovery. Natural gas typically contains a number of components, carbon dioxide being one of the most frequent that is not a hydrocarbon. Most natural gases contain a certain CO_2 content. The CO_2 content is an effective indicator for geologists to understand geochemical processes in natural gases. The starting point for evaluating the regularity of CO_2 enrichment is the source of the gas. Many studies have been conducted to determine where CO_2 first appeared in the atmosphere (Gould et al., 1981; Shang et al., 1990; Tassi et al., 2012; Dai et al., 2016; Mikov et al., 2018). Dai et al. (1996) divided carbon dioxide gas reservoirs into four categories

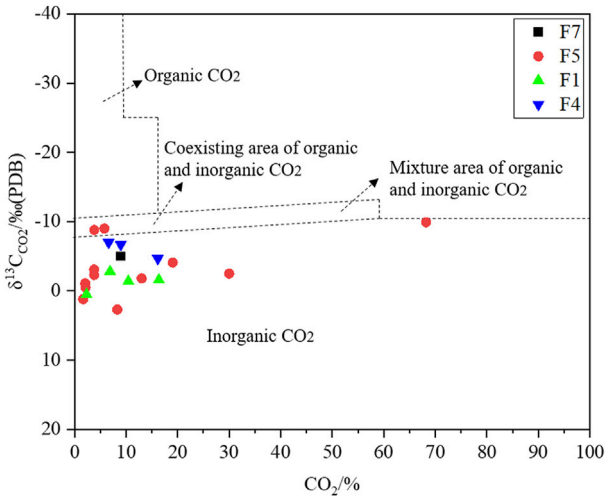

FIGURE 6
Plot of $\delta^{13}C_{CO2}$ vs. CO_2 content of natural gases from the Shunbei area (Modified from Dai et al., 1996).

according to the content of CO_2 in gas reservoirs, and believed that the content of CO_2 in gas reservoirs is more than 60%, CO_2 is of inorganic origin, and the content of CO_2 is 15%–60% Mainly of inorganic origin. There is little difference about CO_2 content in Shunbei area. Most of wells have been acidified fracturing in Shunbei, CO_2 content will be increase during the process of acidizing fracturing. The CO_2 produced by the dissolution of acid in the formation water of carbonate rocks is generally low in formation rate and gas production intensity, because the acid in the formation water is generally low in content and concentration. However, the high concentration and quantity of strong acid injected during artificial acid fracturing can quickly react with the carbonate formation to produce a large amount of CO_2 in a short period of time, resulting in high CO_2 content in gas samples collected during this period (Zhang et al., 2010). Therefore, the CO_2 content were related to acidified fracturing in Shunbei. Carbon dioxide origin can be determined by measuring its $\delta^{13}C$ isotope signature, which has been shown to be greater than −8% for inorganic carbon dioxide and less than −10% for organic carbon dioxide (Dai et al., 1996). Figure 6 shows that the majority of the CO_2 in natural gases in the Shunbei region comes from inorganic sources and exists in a coexisting zone.

5.3 Identification of kerogen cracking gas and oil cracking gas

For a complete picture of the natural gas cycle and its origin, it is also important to distinguish between oil-associated gas and coal-type gas, as well as kerogen cracking gas and oil cracking gas (Tissot et al., 1984; Lan et al., 2009; Cheng et al., 2013). If the natural gas is oil cracking gas, then the oil and gas that the source rock produces during the peak phase of oil generation are in the large cracking gas stage when they are trapped to form paleo-reservoirs. Since the oil reservoir created in the early stage of the source rock would have been destroyed, the availability of

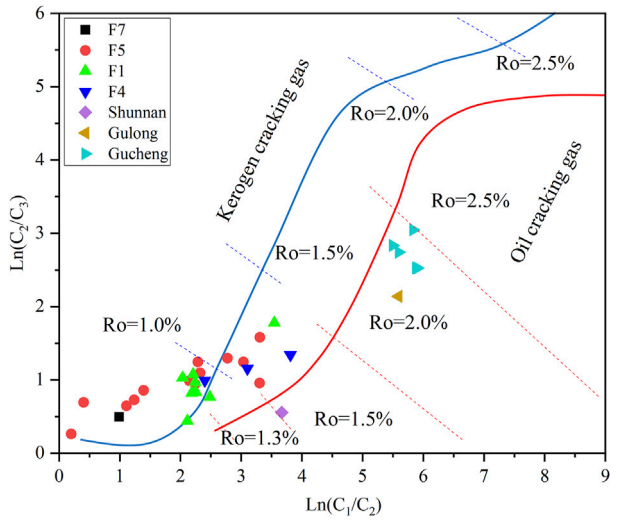

FIGURE 7
The diagram of ln (C_1/C_2) *versus* ln (C_2/C_3) for source identification of natural gases: kerogen cracking and oil cracking (Modified from Berner et al., 1996; Huang B. J. et al., 2016; Stahl et al., 1975).

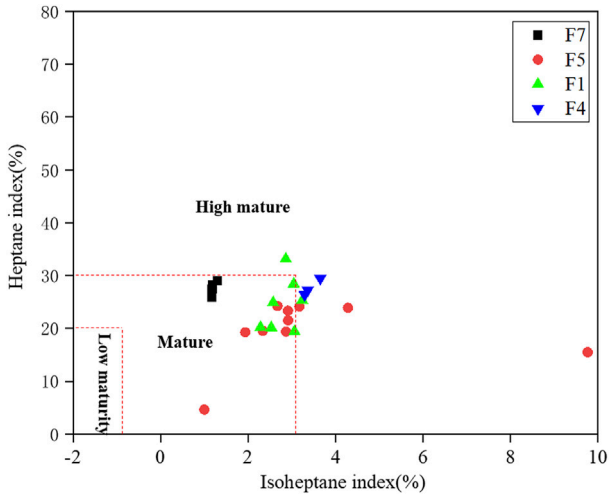

FIGURE 8
The relationship between the heptane index and the iso-heptane index of natural gases in Shunbei area (Modified from Thompson 1979).

natural gas would be drastically impacted if it were determined to be kerogen cracking gas (Stahl et al., 1975; Berner et al., 1996; Huang J. et al., 2016). Zhao et al. (2001) proved that there are two kinds of cracking gas in the Tarim Basin, namely, the natural gas in the eastern Tabei Uplift is mainly kerogen cracking gas, and the natural gas in the Hetianhe gas field is mainly crude oil cracking gas; Zhang et al. (2011) proposed that the natural gas in the east Lungu area was mainly crude oil cracking gas.

The natural logarithmic relationship of methane, ethane, and propane ratios shows a positive trend for this ln (C_1/C_2) and ln (C_2/C_3) (Figure 7) (Li et al., 2017). The results show that the values of ln(C_1/C_2) of natural gas in Shunbei area range from 0.20 to 3.81, and the values of ln(C_2/C_3) vary from 0.26 to 1.78, which mainly fall on the evolution curve of kerogen cracking gas, most of which are below 1.5%. Some natural gas is located between the curves of kerogen cracking gas and oil cracking gas, which indicates the contribution of natural gas mixed with oil cracking gas. However, the ln(C_1/C_2) values of natural gas in Shunnan, Gulong and Gucheng areas are mostly greater than 4, and the ln(C_2/C_3) values vary greatly, ranging from 0.5 to 3.04, which falls on the evolution curve of crude oil cracking gas. The maturity of natural gas is mostly between 1.5% and 2.5% (Ma et al., 2021).

From Shunbei to Shuntuo to Shunnan area, the content of methyl adamantane in crude oil shows an increasing trend, which indicates that the cracking degree of crude oil has increased, which provides geochemical evidence that the natural gas is crude oil cracking gas in Shuntuo and Shunnan areas (Ma et al., 2021). The oil cracking degree of Well Shuntuo 1 and Well Shunnan 1 are 96%, 98%, respectively (Ma et al., 2021). The coke bitumen developed in the Ordovician Yingshan Formation reservoir in Shunnan, Gulong and Gucheng area provides petrological evidence for the formation of natural gas as crude oil cracking gas in this area. The high vitrinite reflectance of pyrobitumen indicates a high degree of cracking of the paleo-oil reservoir (Cao et al., 2019; Zhou et al., 2019).

5.4 Thermal maturity of natural gas

Since the thermal maturity of natural gas cannot be directly obtained, it is necessary to use its carbon isotope to judge. Methane carbon isotopes in natural gas are closely related to maturity. Important theoretical support for tracing the gas's origins and establishing a gas-source correlation comes from a set of empirical carbon isotope-maturity relationships given for evaluating the maturity of gases and estimated Ro value (Dai, 1989; Huang et al., 1996). There are some discrepancies between the calculated conclusions of the $\delta^{13}C$-maturity models in the Shunbei, however, because of the region's varied geological settings and/or accumulation history. Because of this, Huang (1979) advocated using the $\delta^{13}C$-maturity model, with the equation $\delta^{13}C_1 = 21.88\log Ro - 45.6$ (Huang et al., 1996). The $\delta^{13}C_1$-Ro model was used to calculate the Ro values (Table 1). The carbon isotope of methane and Ro values are displayed in Table 1 in accordance with the dryness coefficient, demonstrating that the maturity of natural gases in the Shunbei area steadily increases from west to east. The southern part of Fault 5 has a higher maturity level than the center and northern parts. The northern portion of Fault 1 is more mature than the southern portion. Natural gas maturity can be determined using a variety of markers, the most popular and reliable of which is the light hydrocarbon component. The light hydrocarbon component's n- and iso-heptane may efficiently discriminate between various maturity stages (Thompson, 1979). Figure 8 shows that the natural gas in Shunbei area is in the mature to high mature stage.

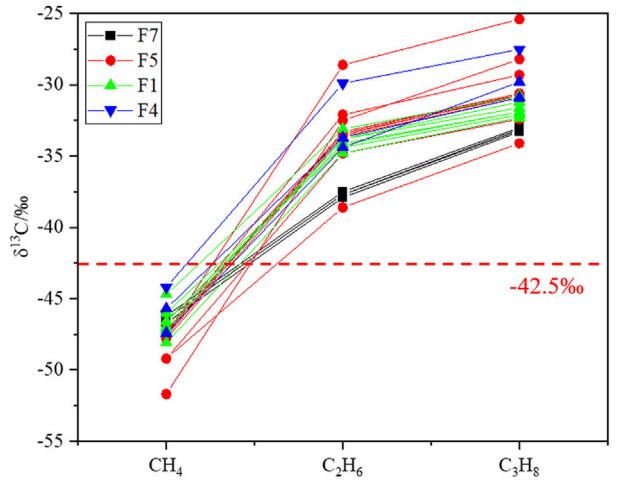

FIGURE 9
Carbon isotopic series of alkane gas in the Tarim Basin.

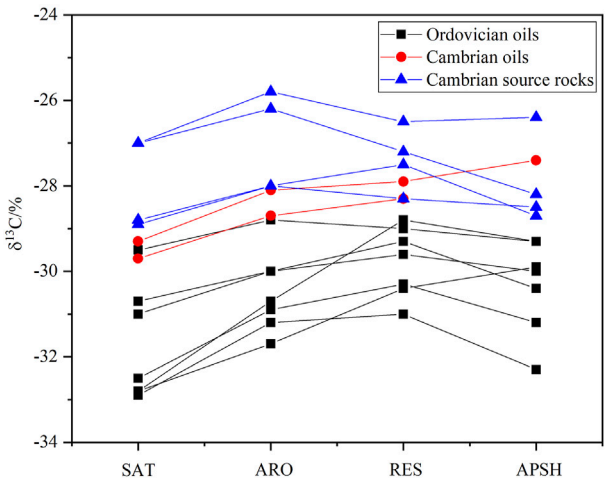

FIGURE 10
Carbon isotope curves of non-hydrocarbon from the Tarim Basin.

5.5 Source of natural gas

It is common knowledge that the Cambrian, Lower-Middle Ordovician, and Upper Ordovician were the most productive times for production of the marine source rocks that make up the Tarim Basin (Zhang et al., 2000b). While both the Xishanbulake-Xidashan and Yuertusi Formations contributed to the formation of Cambrian source rocks, the Yuertusi Formation was far more instrumental. Well XH1 uncovered the Cambrian Yuertusi Formation, which has a total thickness of about 40 m and a total organic carbon (TOC) concentration of 1.0%–9.43% (7 samples averaged out to 5.5%) (Yun et al., 2014; Jin et al., 2017). Type I-II organic compounds make up the bulk of all organic materials (Xiao et al., 2000). There is now a stage of extreme maturity in the Cambrian source rocks (Zhan, 2016).

The Heituao and Saergan Formations have the highest concentration of middle and lower Ordovician source rocks (Chen et al., 2014). The presence of kerogen type II in algae and acritarchs causes a wide range of total organic carbon (TOC) values in Middle-Lower Ordovician source rocks (average 1.77%; 7 samples) (Zhao et al., 2012; Zhao et al., 2014). There is a total organic carbon concentration of 0.47–0.56% in the Upper Ordovician source rocks of the North Uplift of the Tarim Basin, and a TOC concentration of 0.5% or higher in rocks with a thickness of 6–28 m. Natural gas in the Shunbei area was determined to be oil-associated gas based on its geochemical features and those of the source rocks. The Ordovician age is largely responsible for the generation of the gas found in oil reservoirs. The evidence is broken down and addressed in detail below.

①The $\delta^{13}C$ properties of the natural gas in the Shunbei exploratory wells show that the oil-associated gas originates from the Ordovician source rocks. Gaseous alkanes from the Middle-Upper Ordovician and Cambrian have been dated using their carbon isotope distribution curves, which have been published by Wang et al. (2014). It is discovered that the wet gases show steep C_1-C_3 alkane carbon isotope distribution curves with negative $\delta^{13}C_1$ values (<− 42.5‰), which are assumed to have originated from Middle-Upper Ordovician source rocks. In contrast, Cambrian natural gas had $\delta^{13}C$ values that were considerably high (>−42.5‰), along with flat distribution curves for carbon isotopes C_1–C_3. Therefore, using the carbon isotopes of gaseous alkanes permits one to determine the origin of gases and establish relationships between gases. The wet gas from the Shunbei correlates well with gases from the Middle-Upper Ordovician, with $\delta^{13}C$ values that range from 44‰ to 52‰ (or <− 42.5‰) and a steep distribution curve of C_1-C_3 alkanes carbon isotopes (Table 1; Figure 9).

②In accordance with the inheritance of isotopes, dispersion of isotopes, and variation of isotopes during the formation and evolution of hydrocarbons, the carbon isotopes can be utilized to correlate oil sources. The majority of Cambrian source rock samples exhibit stable carbon isotopes heavier than −30‰, with the greatest values seen in Well H4 at −25.8‰. The isotopic curve distribution of Cambrian and Ordovician crude oils is shown in Figure 10 and Table 2. Obviously, Cambrian crude oils are consistent with Cambrian source rocks. On the other hand, the isotopes of Ordovician crude oil are obviously lighter and are distributed in −32‰ ~ −36‰ (Song et al., 2016), so it is obviously impossible for them to be derived from Cambrian source rocks.

5.6 Oil and gas accumulation and enrichment patterns

The crude oil in Shunbei area mainly comes from the Lower Cambrian Yuertusi Formation source rocks (Yun et al., 2014), the Ordovician reservoir is mainly controlled by the multi-stage structural rupture of the strike-slip fault zone and the dissolution along the fault (Jiang et al., 2005). The characteristics of hydrocarbon reservoirs revealed in shallow and deep parts of the same fault zone are consistent. For example, deep well SHB1-10H and shallow well SHB1-3 of Shunbei No. 1 fault zone have basically the same crude oil density and gas dryness coefficient of the two Wells, which

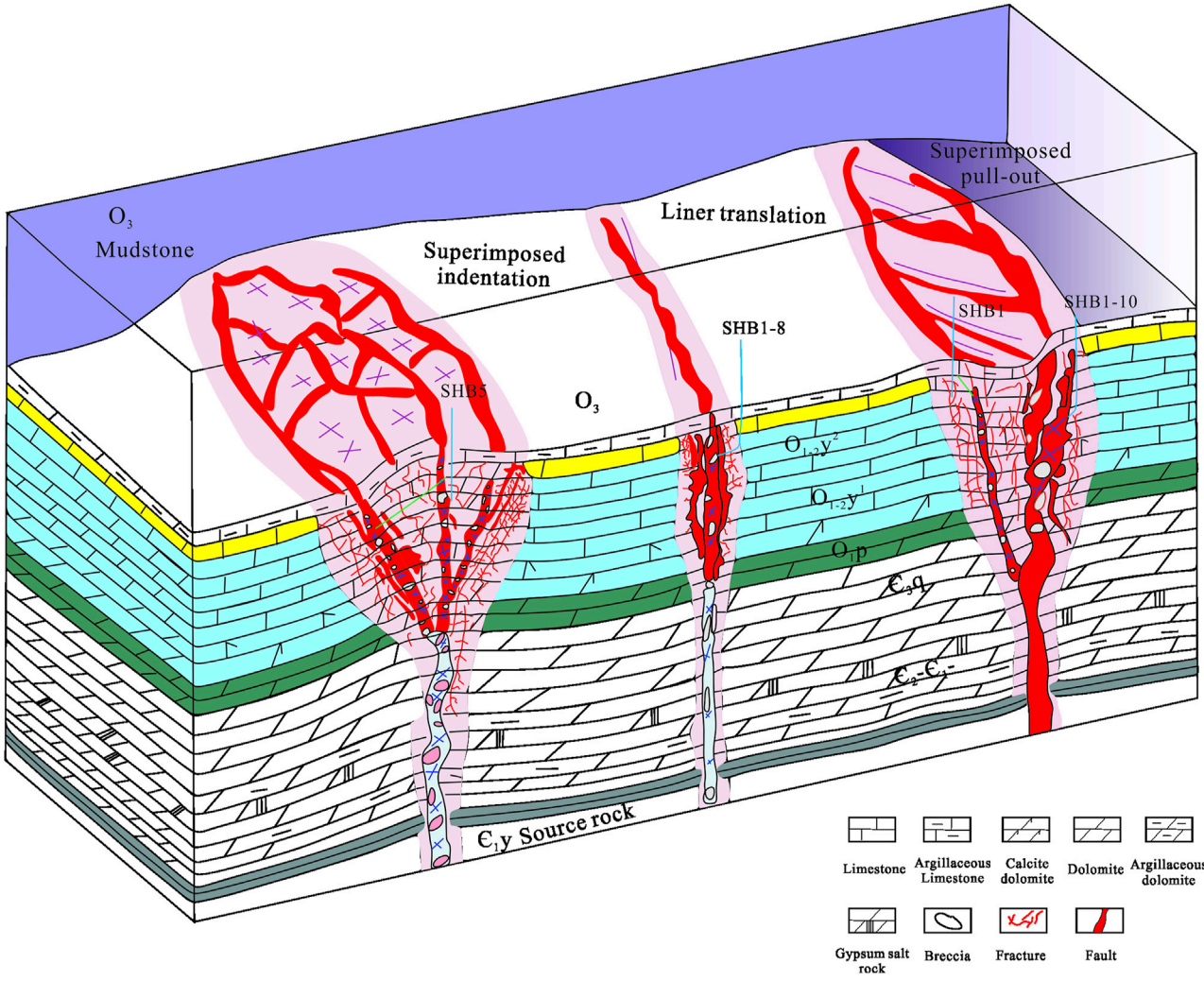

FIGURE 11
Oil and gas accumulation and enrichment patterns of different segments of strike slip fault zone in Shunbei Oilfield (Modified from Qi 2021).

proves that the oil and gas generated by *in-situ* source rock is mainly formed by vertical transport along the fault in Shunbei area. The movable oil and gas are mainly accumulated since the late Hercynian period, and the fault zone plays an obvious role in controlling reservoir and accumulation. This area is located in the sedimentary area of gentle slope source rocks in the early Cambrian period. In the later period, the pass-source strike-slip fault was developed and the reservoir was dominated by "fault-karst". Therefore, because strike slip faults influence in-reservoir geochemical processes and vertical petroleum migration, strike slip faults play an important role in the ultra-deep fault-karst petroleum systems present in the Shunbei area (Figure 11) (Qi, 2021).

6 Conclusion

In the Shunbei area, the natural gas is the origin of oil-associated gas and its parent material type is I kerogen. The relationship between carbon number 1/n and natural gas δ^{13}Cn can be further subdivided into I_1, I_2 and I_3 subclasses. The $\delta^{13}C_1$ and $\delta^{13}C_2$ values for Type I_1 gases are highly enriched at $\delta^{13}C$, ranging from −47.5‰ to −44.2‰ (−45.85‰ on average) and −28.6‰ to −29.9‰ (−29.3‰ on average), respectively. However, Type I_2 and Type I_3 gases have higher $\delta^{13}C$ depletion levels than Type I_1 gases.

Inevitably, the natural gas in the Shunbei area was dominated by oil-associated gas, as shown by modified $\ln C_1/C_2$ vs. $\ln C_2/C_3$ plots, and oil cracking gas is present in the natural gas mixture. Carbon isotope ratios of the source rocks, natural gas, and oil in the Shunbei area suggest that the gases originated in the Ordovician source rocks.

The fault zone in the Shunbei area can be shown to control accumulation within reservoirs. As a new type of reservoir, ultra-deep fault-karst reservoir in the Shunbei area extended the theory of hydrocarbon accumulation in marine carbonates, shows a great exploration potential of ultra-deep marine

carbonate formations, and is an important field for reserve increase in the future.

Data availability statement

The datasets presented in this study can be found in online repositories. The names of the repository/repositories and accession number(s) can be found in the article/Supplementary Material.

Author contributions

Conceptualization, DH; methodology, ZJ; software, XZ and JB; review and editing, XM and ZJ.

Funding

The work was supported by project No. 202107ZB0123.

Acknowledgments

All data and samples were generously provided by Northwest Oilfield Company, SINOPEC, which the authors gratefully acknowledge.

Conflict of interest

XZ was employed by the company Northwest Oilfield Company.

The remaining authors declare that the research was conducted in the absence of any commercial or financial relationships that could be construed as a potential conflict of interest.

Publisher's note

All claims expressed in this article are solely those of the authors and do not necessarily represent those of their affiliated organizations, or those of the publisher, the editors and the reviewers. Any product that may be evaluated in this article, or claim that may be made by its manufacturer, is not guaranteed or endorsed by the publisher.

References

Bai, G. P., and Cao, B. F. (2014). Global deep oil and gas reservoirs and their distribution. *Oil Gas. Geol.* 35 (1), 19–25. (in Chinese with English abstract). doi:10.11743/ogg20140103

Bernard, B. B., Brooks, J. M., and Sackett, W. M. (1978). Light hydrocarbons in recent Texas continental shelf and slope sediments. *J. Geophys. Res.* 33, 4053–4061. doi:10.1029/JC083iC08p04053

Berner, U., and Faber, E. (1996). Empirical carbon isotope/maturity relationships for gases from algal kerogens and terrigenous organic matter, based on dry, open-system pyrolysis. *Org. Geochem.* 24, 947–955. doi:10.1016/S0146-6380(96)00090-3

Cao, Y. H., Wang, S., Zhang, Y. J., Yang, M., Yan, L., Zhao, J. L., et al. (2019). Petroleum geological conditions and exploration potential of Lower Paleozoic carbonate rocks in Gucheng area, Tarim, China. *Petrol. explor. Dev.* 46 (6), 1099–1114. doi:10.11698/PED.2019.06.08

Chen, H. H., Wu, Y., Feng, Y., Lu, Z. Y., Hu, S. Z., Yun, L., et al. (2014). Timing and chronology of hydrocarbon charging in the ordovician of tahe oilfield, Tarim Basin, NW China. *Oil Gas. Geol.* 35 (6), 806–819. doi:10.11743/ogg20140608

Chen, Q. L., Yang, X., Chu, C. L., Hu, G., Shi, Z., Jiang, H. J., et al. (2015). Recognition of depositional environment of Cambrian source rocks in Tarim Basin. *Oil Gas. Geol.* 06, 880–887. doi:10.11743/ogg20150602

Cheng, H. G., Wei, G. Q., Ran, Q. G., Wu, D. M., Liu, L. W., Xiao, Z. Y., et al. (2013). Relationship between hydrocarbon accumulation and solid bitumen characteristics of the Lower Paleozoic in the eastern Tarim Basin. *Nat. Gas. Ind.* 33 (10), 40–46. doi:10.3787/j.issn.1000-0976.2013.10.006

Chung, H. M., Gormly, J. R., and Squires, R. M. (1988). Origin of gaseous hydrocarbons in subsurface environments: Theoretical considerations of carbon isotope distribution. *Chem. Geol.* 71, 97–104. doi:10.1016/0009-2541(88)90108-8

Dai, J., Ni, Y., Zhang, W., Huang, S., Gong, D., Liu, D., et al. (2016). Relationships between wetness and maturity of coal–derived gas in China. *Petrol. explor. Dev.* 43 (5), 737–739. doi:10.1016/S1876-3804(16)30088-X

Dai, J. X. (1989). Composition characteristics and origin of carbon isotope of liuhuanantan natural gas in tengchong county, Yunan Province. *China Sci. Bull.* 34, 690–692.

Dai, J. X., Song, Y., Dai, C. S., and Wang, D. R. (1996). Geochemistry and accumulation of carbon dioxide gases in China. *AAPG Bull.* 80, 1615–1626. doi:10.1306/64EDA0D2-1724-11D7-8645000102C1865D

Dai, J. X., Zou, C. N., Liao, S. M., Dong, D. Z., Ni, Y. Y., Huang, W. H., et al. (2014). Geochemistry of the extremely high thermal maturity longmaxi shale gas, southern Sichuan basin. *Org. Geochem.* 74, 3–12. doi:10.1016/j.orggeochem.2014.01.018

Deng, S., Li, H. L., Zhang, Z. P., Zhang, J. B., and Yang, X. (2019). Structural characterization of intracratonic strike-slip faults in the central Tarim Basin. *AAPG Bull.* 103 (1), 109–137. doi:10.1306/06071817354

Dutton, S. P., and Loucks, R. G. (2010). Diagenetic controls on evolution of porosity and permeability in lower Tertiary Wilcox sandstones from shallow to ultradeep (200–6700m) burial, Gulf of Mexico Basin, U.S.A. *Mar. Petrol. Geol.* 27 (1), 69–81. doi:10.1016/j.marpetgeo.2009.08.008

Gould, K. W., Hart, G. H., and Smith, J. W. (1981). Carbon dioxide in the southern coalfields a factor in the evaluation of natural gas potential. *Proceedings– Australasisn Inst. Min. Metall.* 279, 41–42.

He, D. F., Zhou, X. Y., and Yang, H. J. (2008). Formation mechanism and tectonic types of intracratonic paleo–uplifts in the Tarim Basin. *Ear. Sci. Fron.* 15 (2), 207–221.

Huang, B. J., Tian, H., Li, X. S., Wang, Z. F., and Xiao, X. M. (2016). Geochemistry, origin and accumulation of natural gases in the deepwater area of the Qiongdongnan Basin, South China Sea. *Mar. Petrol. Geol.* 72, 254–267. doi:10.1016/j.marpetgeo.2016.02.007

Huang, D. F., Liu, B. Q., Wang, T. D., Xu, Y. C., Chen, S. J., and Zhao, M. J. (1996). Genetic types and maturity identification of natural gas in Eastern Tarim Basin. *Sci China Ser. D.* 36 (4), 365–372. doi:10.1016/S0009-2541(99)00053-4

Huang, J., Ye, D. L., and Han, Yu. (2016). Petoleum geology features and accumulation controls for ultra-deep oil and gas reservoirs. *Pet. Geo. Exp.* 5 (38), 635–640. (in Chinese with English abstract). doi:10.11781/sysydz201605635

Jia, C. Z., and Pan, X. Q. (2015). Research processes and main development directions of deep hydrocarbon geological theories. *Acta Pet. Sin.* 36 (12), 1457–1469. doi:10.7623/syxb201512001

Jia, C. Z. (1997). Tectonic Characteristics and Petroleum of Tarim Basin China. *Petrol. Ind. beijing.* 1997, 205–389. (in Chinese with English abstract).

Jiao, F. Z. (2018). Significance and prospect of ultra-deep carbonate fault-karst reservoirs in Shunbei area, Tarim Basin. *Oil Gas. Geol.* 39 (02), 208–216. doi:10.11743/ogg20180201

Jin, Z. J., Liu, Q. Y., Yun, J. B., and Tenger, B. (2017). Potential petroleum sources and exploration directions around the Manjar Sag in the Tarim Basin. *Sci. Chi. Ear. Scie.* 2, 235–245. doi:10.1007/s11430-015-5573-7

Lan, X. D., Zhu, Y. M., Rang, Q. G., and Cheng, H. G. (2009). A discussion on the geochemical characteristics and migration and accumulation of natural gas in the eastern Tarim Basin. *Pet. Geol. Exp.* 30 (3), 324–329.

Li, J., Li, Z. S., Wang, X. B., Wang, D. L., Xie, Z. Y., Li, J., et al. (2017). New indexes and charts for Genesis identification of multiple natural gases. *Pet. Explor. Dev.* 44 (4), 535–543. doi:10.1016/S1876-3804(17)30062-9

Li, J. Z., Tao, X. W., Bai, B., Huang, S. P., Jiang, Q. C., Zhao, Z. Y., et al. (2021). China's marine ultra-deep oil and gas geological conditions, accumulation evolution and favorable exploration direction. *Pet. Geol. Exp.* 48 (1), 52–67. doi:10.11698/PED.2021.01.05

Ma, A. L., He, Z. L., Yun, L., Wu, X., Qiu, N. S., Chang, J., et al. (2021). The geochemical characteristics and origin of Ordovician ultra–deep natural gas in the North Shuntuoguole area, Tarim Basin, NW China. *Nat. Gas. Geosci.* 32 (7), 1047–1060. doi:10.11764/j.issn.1672-1926.2021.03.012

Ma, N. B., Jin, S. L., Yang, R. Z., Meng, L. B., Wang, L., and Hu, Y. Z. (2019). Seismic response characteristics and identification of fault-karst reservoir in Shunbei area, Tarim basin. *Oil. Geo. Pros.* 54 (2), 398–403. doi:10.13810/j.cnki.issn.1000-7210.2019.02.019

Ma, Y. S., Li, M. W., Cai, X. Y., Xu, X. H., Hu, D. F., Qu, S. L., et al. (2020). Mechanisms and exploitation of deep marine petroleum accumulations in China: Advances, technological bottlenecks and basic scientific problems. *Oil Gas. Geol.* 41 (4), 655683. (in Chinese with English abstract).

Mikov, A. V., and Etiope, G. (2018). revised genetic diagrams for natural gases based on a global dataset of > 20,000 samples. *Org. Geochem.* 125, 109–120. doi:10.1016/j.orggeochem.2018.09.002

Ni, Y. Y., Liao, F. R., Gao, J. L., Chen, J. P., Yao, L. M., and Zhang, D. J. (2019). Hydrogen isotopes of hydrocarbon gases from different organic facies of the Zhongba gas field, Sichuan Basin, China. *J. Petrol. Sci. Eng.* 179, 776–786. doi:10.1016/j.petrol.2019.04.102

Pan, J. P., and Jiao, Z. L. (2022). Study on China's development strategy for oil & gas industry toward the goal of carbon peaking and carbon neutrality. *Tra. For.* 30 (8), 01–15. (in Chinese with English abstract).

Pang, X. Q., Wang, W. Y., Wang, Y. Y., and Wu, L. Y. (2015). Comparision of otherness on hydrocarbon accumulation conditions and characteristics between deep and middle-shallow in petroliferous basins. *Acta Petro Sin.* 36 (10), 1167–1185. doi:10.7623/syxb201510001

Prinzhofer, A., and Huc, A. Y. (1995). Genetic and post−genetic molecular and isotopic fractionations in natural gases. *Chem. Geol.* 126, 281–290. doi:10.1016/0009-2541(95)00123-9

Qi, L. (2021). Structural characteristics and storage control function of the Shun I fault zone in the Shunbei region, Tarim Basin. *J. Petrol. Sci. Eng.* 203, 108653. doi:10.1016/j.petrol.2021.108653

Ren, Z. L., Cui, J. P., Qi, K., Yang, G. L., Chen, Z. J., Yang, P., et al. (2020). Control effects of temperature and thermal evolution history of deep and ultra-deep layers on hydrocarbon phase state and hydrocarbon generation history. *Nat. Gas. Indus (B)* 7 (5), 453–461. doi:10.1016/j.ngib.2020.09.003

Schoell, M. (1980). The hydrogen and carbon isotopic composition of methane from natural gases of various origins. *Geochim. Cosmochim. Acta.* 44, 649–661. doi:10.1016/0016-7037(80)90155-6

Shang, G. Z., and Gao, S. (1990). The CO_2 discharges and earthquakes in Western Yunnan. *Acta Seismol. Sin.* 12, 186–193.

Song, D. F., Wang, T. G., and Li, J. M. (2016). Geochemistry and possible origin of the hydrocarbons from Wells Zhongshen1 and Zhongshen1C, Tazhong Uplift. *Sci. China Earth Sci.* 46, 840–850. doi:10.1007/s11430-015-5226-z

Stahl, W. J., and Carey, J. B. D. (1975). Source-rock identification by isotope analyses of natural gases from fields in the Val Verde and Delaware basins, west Texas. *Chem. Geol.* 16, 257–267. doi:10.1016/0009-2541(75)90065-0

Tassi, F., Fiebig, J., Vaselli, O., and Nocentini, M. (2012). Origins of methane discharging from volcanic−hydrothermal, geothermal and cold emissions in Italy. *Chem. Geol.* 310–311, 36–48. doi:10.1016/j.chemgeo.2012.03.018

Thompson, K. F. M. (1979). Light hydrocarbons in subsurface sediments. *Geochim. Cosmochim. Acta.* 43, 657–672. doi:10.1016/0016-7037(79)90251-5

Tissot, B. T., and Welte, D. H. (1984). *Petroleum Formation and occurrences*. Berlin: Springer.

Wang, T. G., Song, D. F., Li, M. j., Ynag, C. Y., Ni, Z. Y., Li, H. L., et al. (2014). Natural gas source and deep gas exploration potential of the Ordovician Yingshan Formation in the Shunnan-Gucheng region, Tarim Basin. *Oil Gas. Geol.* 12 (06), 753–762. doi:10.11743/ogg20140602

Wang, T. G., Wang, C. J., and Zhang, W. B. (2003). *Geochemical study on formation of the Ordovician oil/gas reservoirs in Tahe oil field*. Beijing, China: Sinopec Xinxing Northwest China Branch.

Wang, X., Liu, W., Shi, B., Zhang, Z., Xu, Y., and Zheng, J. (2015). Hydrogen isotope characteristics of thermogenic methane in Chinese sedimentary basins. *Org. Geochem.* 83-84, 178–189. doi:10.1016/j.orggeochem.2015.03.010

Whiticar, M. J. (1999). Carbon and hydrogen isotope systematics of bacterial formation and oxidation of methane. *Chem. Geol.* 161, 291–314. doi:10.1016/S0009-2541(99)00092-3

Whiticar, M. J., Faber, E., and Schoell, M. (1986). Biogenic methane formation in marine and freshwater environments; CO_2 reduction vs. acetate fermentation; isotope evidence. *Geochim. Cosmochim. Acta.* 50, 693–709. doi:10.1016/0016-7037(86)90346-7

Wu, F. Q., and Xian, X. F. (2006). Current state and countermeasure of deep reservoirs exploration. *Sedi Geol Teth Geol* 26 (2), 68–71. (in Chinese with English abstract).

Xiao, X., Wilkins, R. W. T., Liu, D. H., Liu, Z. F., and Fu, J. M. (2000). Investigation of thermal maturity of lower Palaeozoic hydrocarbon source rocks by means of vitrinite-like maceral reflectance – a Tarim Basin case study. *Org. Geochem.* 31, 1041–1052. doi:10.1016/S0146-6380(00)00061-9

Xie, Z. Y., Li, J., Li, Z. S., Guo, J. Y., Li, J., Zhang, L., et al. (2017). Geochemical characteristics of the upper Triassic Xujiahe formation in Sichuan Basin, China and its significance for hydrocarbon accumulation. *Acta Geol. Sin.* 91, 1836–1854. doi:10.1111/1755-6724.13414

Yang, F. L., Yu, L., Wang, T. G., Ding, Y., and Li, M. J. (2017). Geochemical characteristics of the Cambrian source rocks in the Tarim Basin and oil-source correlation with typical marine crude oil. *Oil Gas. Geol.* 38 (05), 851–861. doi:10.11743/ogg20170503

Yun, J. B., Jin, Z. J., and Xie, G. J. (2014). Distribution of major hydrocarbon source rocks in the Lower Paleozoic, Tarim Basin. *Oil Gas. Geol.* 35, 827–838. doi:10.11743/ogg20140610

Yun, L., and Cao, Z. C. (2014). Hydrocarbon enrichment pattern and exploration potential of the Ordovician in Shunnan area, Tarim Basin. *Oil Gas. Geol.* 35 (6), 788–797. doi:10.11743/ogg20140606

Zhai, G. M., and He, W. Y. (2004). An important petroleum exploration region in Tarim Basin. *Acta Pet. Sin.* 25 (1), 1–7.

Zhai, G. M., Wang, S. H., and He, W. Y. (2012). Hostop trend and enlightenment of global ten-year hydrocarbon exploration. *Acta Pet. sin.* 33, 14–19. (in Chinese with English abstract).

Zhan, Z. W. (2016). *De-convoluting the marine crude oil mixtures in the Tabei uplift, Tarim basim, NW China*. Beijing, China: Guangzhou Institute of Geochemistry, Chinese Academy of Sciences.

Zhang, B. S., Gu, Q. Y., Zhang, H. Z., Zhao, Q., and Yin, F. L. (2010). Genesis and Study Significance of High CO 2 Content in Carbonate Rocks in Tazhong Area, Tarim Basin. *Mari. Ori. Petro. Geol.* 15 (3), 70–73.

Zhang, H., Xiong, Y., Liu, J. Z., Liao, Y. H., and Geng, A. (2005). Pyrolysis kinetics of Pure n−C_{18} H_{38} (I): gaseous hydrocarbon and carbon isotope evolution. *Acta Geol. Sin.* 79, 569–574.

Zhang, S. C., Su, J., Wang, X. M., Zhu, G. Y., Yang, H. J., Liu, K. Y., et al. (2011). Geochemistry of Palaeozoic marine petroleum from the Tarim Basin, NW China: Part 3. Thermal cracking of liquid hydrocarbons and gas washing as the major mechanisms for deep gas condensate accumulations, NW China: Part 3. Thermal cracking of liquid hydrocarbons and gas washing as the major mechanisms for deep gas condensate accumulations. *Org. Geochem.* 42, 1394–1410. doi:10.1016/j.orggeochem.2011.08.013

Zhang, S., Zhang, B., Wang, F., Liang, D., and He, Z. (2000b). Middle-Upper Ordovician: the main source of the oils in the Tarim Basin. Mar. *Oil. Gas. Geo.* 5, 16–22. (in Chinese with English abstract).

Zhang, Z. P., Kang, Y., Lin, H. X., Han, J., Zhao, R., Zhu, X. X., et al. (2021). A study on the reservoir controlling characteristics and mechanism of the strike slip faults in the northern slope of Tazhong uplift, Tarim Basin, China. *Arab. Jour. Geo.* 14 (8), 735–762. doi:10.1007/s12517-021-07076-5

Zhao, J. Z., Zhang, W. Z., Li, J., Cao, Q., and Fan, Y. F. (2014). Genesis of tight sand gas in the Ordos Basin, China. *Org. Geochem.* 74, 76–84. doi:10.1016/j.orggeochem.2014.03.006

Zhao, M. J., Zeng, F. G., Qin, S. F., and Lu, S. F. (2001). Two pyrolytic gases found and proved in Talimu Basin. *Nat. Gas. Indus* 21 (1), 35–39. (in Chinese with English abstract).

Zhao, W. Z., Hu, S. Y., Wang, Z. C., Zhang, S. C., and Wang, T. S. (2018). Petroleum geological conditions and exploration importance of Proterozoic to Cambrian in China. *Pet. Geo. Exp.* 45 (1), 1–14. doi:10.1016/S1876-3804(18)30001-6

Zhao, W. Z., Zhu, G. Y., Su, J., Yang, H. J., and Zhu, Y. F. (2012). Study on the Multi−stage Charging Accumulation Model of Chinese Marine Petroleum: Example from Eastern Lungu Area in the Tarim Basin. *Acta Pet. Sin.* 28 (3), 709–721. (in Chinese with English abstract).

Zheng, J. F. (2018). Significance and Prospect of ultar−deep carbonate fault−karst reservoirs in Shunbei area, Tarim Basin. *Oil Gas. Geol.* 39 (2), 207–216. doi:10.11743/ogg20180201

Zhou, X, X., Lü, X. X., Zhu, G. Y., Cao, Y. H., Yan, L., and Zhang, Z. Y. (2019). Origin and formation of deep and superdeep strata gas from Gucheng-Shunnan block of the Tarim Basin, NW China, NW China. *J. Petrol. Sci. Eng.* 177, 361–373. doi:10.1016/j.petrol.2019.02.059

Zhu, D., Meng, Q., Jin, Z., Liu, Q., and Hu, W. (2015). Formation mechanism of deep Cambrian dolomite reservoirs in the Tarim basin, northwestern China. *Mar. Petrol. Geol.* 59, 232–244. doi:10.1016/j.marpetgeo.2014.08.022

Zhu, G., Milkov, A. V., Chen, F., Weng, N., Zhang, Z., Yang, H., et al. (2018). Non-cracked oil in ultra-deep high-temperature reservoirs in the Tarim basin, China. *Mar. Petrol. Geol.* 89, 252–262. doi:10.1016/j.marpetgeo.2017.07.019

Zou, Y. R., Cai, Y., Zhang, C., Zhang, X., and Peng, P. A. (2007). Variations of natural gas carbon isotope−type curves and their interpretation a case study. *Org. Geochem.* 38 (8), 1398–1415. doi:10.1016/j.orggeochem.2007.03.002